Kinetics of crystal nucleation in undercooled droplets of Sb- and Te-based alloys used for phase change recording

J. A. Kalb[a] and F. Spaepen
Division of Engineering and Applied Sciences, Harvard University, Cambridge, Massachusetts 02138

M. Wuttig
I. Physikalisches Institut der Rheinisch-Westfälische Technische Hochschule (RWTH) Aachen, 52056 Aachen, Germany

(Received 19 May 2005; accepted 27 July 2005; published online 12 September 2005)

Droplets of molten alloys of composition $Ge_{12}Sb_{88}$, $Ag_{0.055}In_{0.065}Sb_{0.59}Te_{0.29}$, $Ge_4Sb_1Te_5$, and $Ge_2Sb_2Te_5$, used for optical data storage, surrounded by a molten dehydrated B_2O_3 flux were undercooled to 40–80 K below their liquidus temperature in a differential thermal analyzer. The crystal-melt interfacial energy was calculated from the nucleation temperature using the classical nucleation theory, which gave values of around 0.20 times the heat of fusion per atom in the interface for all alloys. This value should be a lower limit since we did not establish that nucleation was homogeneous in the experiments. The steady-state nucleation rate was calculated between the liquidus and glass transition temperatures and was higher for the GeSbTe alloys than for the Sb-rich alloys. Nevertheless, the nucleation rates appear too high to allow amorphization under operating conditions for the highest achievable cooling rates. Therefore, we conclude that it is the presence of an incubation time that makes amorphization and therefore phase change recording possible in both optical and electronic media. © *2005 American Institute of Physics*. [DOI: 10.1063/1.2037870]

I. INTRODUCTION

Tellurium- and antimony-based alloys are used for optical data storage in commercial rewritable phase change media. In rewritable compact disks (CDs) and digital video disks (DVDs), a thin film of a Te alloy is locally and reversibly switched by laser heating between the amorphous and the crystalline state. These states can be distinguished optically by their difference in reflectivity.[1] Recently, Te alloys have also shown high potential for future electronic nonvolatile data storage.[2] In these so-called *phase change random access memories* (PC-RAMs), electrical power provides the heat that is necessary for transformations between the amorphous and crystalline states, which can be distinguished subsequently by their pronounced difference in electrical conductivity.[2–5]

To develop programmable resistor elements on the nanometer scale for the next generation of phase change media, it is highly necessary to understand their crystallization kinetics better. Those have been extensively studied on the time scale of minutes[5–9] around the glass transition temperature T_g and are useful to estimate the stability of the amorphous phase against spontaneous recrystallization at room temperature.[10] Unfortunately, quantitative extrapolations of such crystallization parameters to higher temperatures are difficult because the activation energies of the atomic transport coefficients are strongly temperature dependent[11] around T_g. Therefore, such experiments have limited comparability to kinetics under operating conditions. We present estimates of the crystal-melt interfacial energy σ, which is the most important parameter for the calculation of the steady-state nucleation rate, from undercooling liquid droplets of Sb- and Te-based alloys below the liquidus temperature T_l and observing crystallization in a differential thermal analyzer (DTA). That the atomic transport coefficients are only weakly temperature dependent around T_l allows us to make quantitative extrapolations of the nucleation rate to the temperature regime between T_g and T_l over which crystallization may occur under operating conditions.

The undercooling of a droplet is usually limited by the presence of impurities, surface oxides, and container walls that act as heterogeneous crystal nucleants.[12] It has been demonstrated that the undercooling can be significantly increased by surrounding the droplet with a liquid flux, which isolates the droplet from the container walls and eliminates nucleants from the surface of the droplet by dissolution and inclusion.[13–19] As a secondary effect, the flux significantly reduces evaporation of volatile droplets.

II. EXPERIMENTAL TECHNIQUES

B_2O_3 flux was chosen for three reasons: (i) B_2O_3 is chemically more stable than all oxides that can form[20] from elemental Ge, Sb, Te, Ag, and In. (ii)Due to its low glass transition and melting temperature, 275 and 450 °C, respectively,[11,21,22] the viscosity of B_2O_3 is sufficiently low around the liquidus of the phase change alloys to serve as an effective flux. (iii) B_2O_3 is an easy glass former that does not crystallize at any temperature at ambient pressure[23] and thereby provides a liquid or amorphous sample container at all temperatures. As B_2O_3 is hydrophilic, it had to be dehydrated by annealing in a Pt crucible for about 30 min at 1000 °C in air.

A Perkin Elmer/Seiko Pyris Diamond thermogravimetric/differential thermal analyzer (TG/DTA)

[a]Also at I. Physikalisches Institut der RWTH Aachen, 52056 Aachen, Germany; electronic mail: kalb@deas.harvard.edu

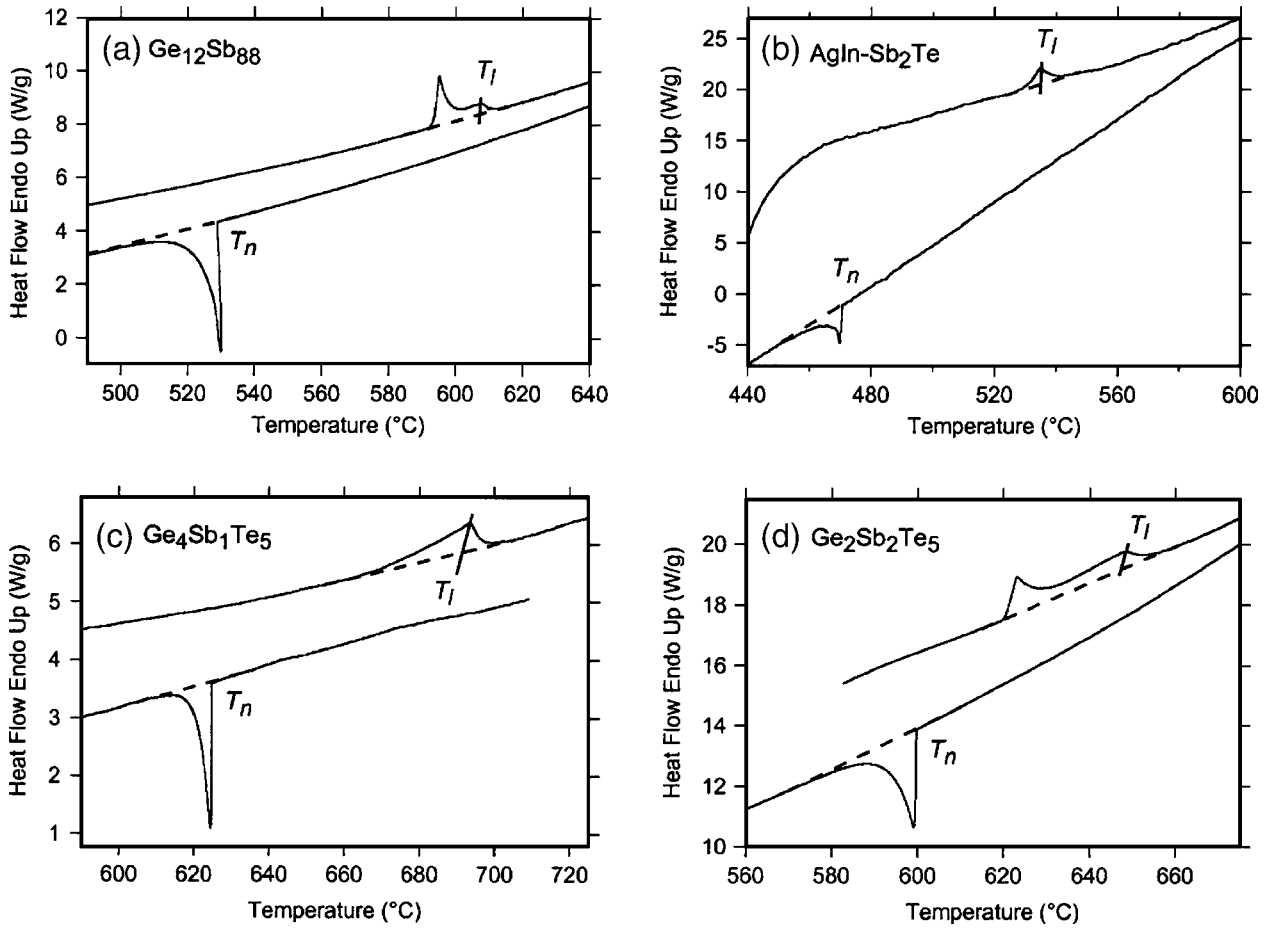

FIG. 1. Heat flow as a function of temperature for B_2O_3-fluxed Sb and Te alloys measured by differential thermal analysis. Heating (upper curve): In order to assign the correct liquidus temperature T_l to the observed endothermic melting peak, an auxiliary line is drawn from the end of the signal to the interpolated base line (dashed) at an angle obtained from a calibration experiment (cf. Ref. 24). Cooling (lower curve): The nucleation temperature T_n is assigned to the onset of the exothermic crystallization peak. Above T_n, the sample remains entirely liquid. For each alloy, the cooling curve displays the *largest* undercooling $\Delta T_n = T_l - T_n$ (cf. Table I) obtained. The heating (cooling) rate was $\dot{T} = \pm 10$ K/min for all alloys, except for $Ge_4Sb_1Te_5$, where it was $\dot{T} = \pm 5$ K/min.

was calibrated[24–27] for both the heating and cooling mode using the melting points and enthalpies of fusion of indium, tin, zinc, and aluminum as standards.

Crystalline bulk samples of the slightly off-eutectic[28] composition $Ge_{12}Sb_{88}$ were prepared by alloying 5N elemental Ge and Sb powders in an argon atmosphere (preevacuated to high vacuum) for 3 h at 1050 °C. After cooling, optical microscopy revealed the eutectic microstructure of 5-μm-thick lamellae. Crystalline bulk samples of compositions $Ag_{0.055}In_{0.065}Sb_{0.59}Te_{0.29}$ (similar in composition to the material of choice in DVD+RW and DVD−RW, hereafter AgIn−Sb_2Te), $Ge_4Sb_1Te_5$, and $Ge_2Sb_2Te_5$ (the material of choice in DVD-RAM) were prepared by cutting chunks from a single sputter target with a razor blade. A typical sample of size between 0.03 and 1 mm^3, determined from its mass and density,[3,5,29] was placed into a cylindrical ceramic DTA sample pan (diameter and height: 5 mm) and surrounded with dehydrated amorphous B_2O_3 chunks at room temperature, which provided a liquid sample container once the pan was heated.

The fluxed sample was repeatedly cycled in the DTA in Ar atmosphere at constant heating and cooling rates between 0.1 and 50 K min^{-1}. Melting upon heating and crystallization upon cooling was observed by an endothermic and an exothermic peak, respectively. The objective of this experiment was to undercool the sample as far as possible and thereby to approach the limit of homogeneous nucleation, which yields the largest possible undercooling. The amount of undercooling as a function of fluxing time t_f and fluxing temperature $T_f > T_l$ was investigated.

A power-compensated differential scanning calorimeter (DSC, Perkin Elmer, Pyris 1), calibrated using the melting points and enthalpies of fusion of indium and zinc, was used to measure the heat of fusion ΔH_f of $Ge_{12}Sb_{88}$, AgIn−Sb_2Te, and $Ge_2Sb_2Te_5$ from the area under the endothermic melting peak upon heating. Due to its high liquidus temperature, the heat of fusion of $Ge_4Sb_1Te_5$ could not be measured in the DSC and had to be estimated from the area of the endothermic DTA peak.

III. RESULTS

The upper curves in Fig. 1 display the endothermic melting peak for all alloys measured in the DTA. Analysis of the melting peak of $Ge_{12}Sb_{88}$ based on the binary phase diagram[28] confirms that this composition is slightly off-eutectic (sharp peak from eutectic melting at 592 °C, followed by a broader peak up to the liquidus of the noneutectic

TABLE I. Liquidus temperature T_l upon heating, lowest nucleation temperature T_n observed upon cooling, largest undercooling $\Delta T_n = T_l - T_n$, and largest relative undercooling $\Delta T_{n,r} = \Delta T_n / T_l$, from differential thermal analysis measurements (cf. Fig. 1). The uncertainty for the temperature is ±1 °C. Calculated lower limit for the crystal-melt interfacial energy σ [absolute value, Eq. (A2)] and α [normalized value, Eq. (A4)] and normalized entropy of fusion β from differential scanning calorimetry (DSC) and differential thermal analysis (DTA) measurements [Eq. (A4)].

Alloy	T_l (°C)	T_n (°C)	ΔT_n (°C)	$\Delta T_{n,r}$	σ (mJ/m^2)	α	β
$Ge_{12}Sb_{88}$	607.0	529.9	77.1	0.088	76±5	0.20±0.01	2.94±0.04[a]
AgIn−Sb_2Te	534.1	471.9	62.2	0.077	55±4	0.19±0.01	2.49±0.05[a]
$Ge_4Sb_1Te_5$	690.7	625.1	65.6	0.068	47±6	0.22±0.01	1.51±0.18[b]
$Ge_2Sb_2Te_5$	643.2	600.7	42.5	0.046	40±3	0.16±0.01	1.93±0.10[a]

[a]From DSC measurements.
[b]From DTA measurements.

phase). The eutectic composition is $Ge_{15}Sb_{85}$ (Ref. 28). For AgIn−Sb_2Te, the measured value for T_l (cf. Table I) is close to the literature value[28] of T_l=545 °C for the alloy Sb_2Te, which is similar in composition to AgIn−Sb_2Te. The measured liquidus temperatures (Table I) for $Ge_4Sb_1Te_5$ and $Ge_2Sb_2Te_5$ agree with other DTA studies.[30–32]

Fluxing the sample slightly above the liquidus gave almost no undercooling for all alloys (about 10 K), no matter how long the fluxing time t_f was. The undercooling is measured from the liquidus, i.e., $\Delta T_n = T_l - T_n$, where T_n is the onset of the exothermic crystallization peak upon cooling (cf. Fig. 1). This is empirically justified by observations that the composition dependence of T_n in undercooling experiments on binary alloy droplets roughly parallels the liquidus line.[33–37] Increasing the fluxing temperature T_f enhanced the undercooling, i.e., B_2O_3 acted as a more efficient flux at higher temperatures, probably due to its viscosity decrease or to the enhanced dissolution kinetics. Fluxing temperatures T_f above about 800 °C did not further enhance the undercooling for any of the alloys. The fluxing time t_f did not have a significant effect on the amount of undercooling. Fluxing times of a few minutes and of a few hours gave the same undercooling for the same fluxing temperature.

The lower curves in Fig. 1 display the exothermic crystallization peak of the cooling cycles that yielded the largest undercooling (cf. Table I). The undercooling was independent of cooling rate and sample volume within the limits mentioned in Sec. II.

After cooling down to room temperature, the samples were exposed by boiling the sample pan in water and thereby dissolving the glassy B_2O_3. Optical microscopy revealed the eutectic microstructure of 5-μm fine lamellae for the $Ge_{12}Sb_{88}$ alloy.

The heat of fusion ΔH_f determined from DSC and DTA measurements has been normalized to an entropy of fusion β according to Eq. (A4) in the Appendix and is given in Table I.

IV. ANALYSIS

The interfacial energy σ was calculated using the method described in the Appendix, with $f(\theta)$ set to unity. Hence, we assume that the largest observed undercooling ΔT_n (Table I) corresponds to homogeneous nucleation. An estimate of the Gibbs free energy difference ΔG between undercooled liquid and crystal based on liquid heat-capacity measurements is available only for AgIn−Sb_2Te due to the higher liquidus temperature for the other alloys.[38] Figure 2 compares the experimental curve of Ref. 38 with the calculations of Eq. (A3) for this alloy. Only the Thompson/Spaepen[39] (TS) and Hoffman[40] (HM) approximations describe the measured curve satisfactorily, but not the Turnbull[41] (TB) approximation, which is usually used only for undercooling of metals, for which the difference in specific heat between liquid and crystal near the melting point is close to zero. We therefore assume that the TS and HM approximations also apply to the other alloys. For small undercoolings $\Delta T_{n,r}$ of less than 10% as given in Table I, the viscosity η can be assumed independent of temperature.[42] Viscosity data around the liquidus temperature are not available for any of the alloys studied here. We therefore estimate the viscosity to be $\eta \sim 2 \times 10^{-2}$ poise, a value measured around the liquidus for $Sb_{100-x}Te_x$, where x ranged from 0 to 100,[43] as well as for $Ge_{100-x}Te_x$, where x ranged from 50 to 100,[44] and also for various other binary Te alloys.[43,45] The uncertainty for the calculated interfacial energy σ in Table I

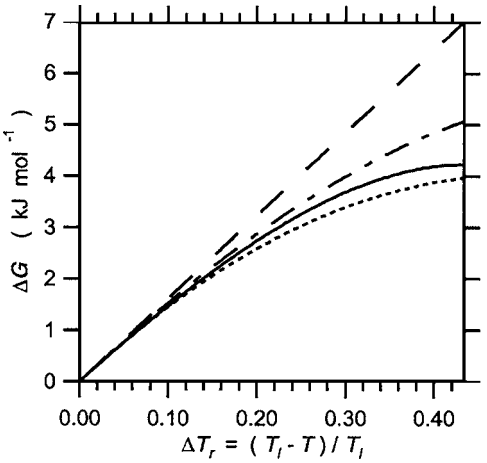

FIG. 2. Difference in molar Gibbs free energy ΔG between the undercooled liquid and the crystal as a function of relative undercooling ΔT_r for AgIn−Sb_2Te. The solid curve is based on liquid heat-capacity measurements from Ref. 38. The other curves are calculated from Eq. (A3) using values for β and T_l given in Table I: Turnbull approximation (TB, dashed), Thompson/Spaepen approximation (TS, dot-dashed), and Hoffman approximation (HM, dotted).

includes (a) the uncertainty in the heat of fusion ΔH_f used for the approximation of ΔG [Eq. (A3)], (b) the uncertainty on the choice of the TS or the HM approximation, and (c) the uncertainty in the factor J_0 [Eq. (A2)], which is two to four powers of 10.[46] Since the dependence of the exponential term in Eq. (A2) on σ is so strong, the value of σ required to satisfy Eq. (A1) is insensitive to the large uncertainty in J_0. The normalized interfacial energy α [Eq. (A4), Table I] is slightly lower for $Ge_2Sb_2Te_5$ than for the other three alloys. All values are smaller than the value $\alpha=0.34\pm0.05$, which was measured for silicon by the same technique,[17] and far smaller than the values obtained by interface modeling for the closest-packed surfaces in pure metals ($\alpha=0.86$ for the face-centered-cubic and hexagonal-closed-packed structures[47] and $\alpha=0.71$ for the body-centered crystal structure[48]). The values of the interfacial energies σ and α in Table I are lower limits, since we did not establish that nucleation was homogeneous in our experiments. If, as is likely, the observed nucleation was heterogeneous, larger undercoolings should be possible. The corresponding values of σ and α would be larger.

To extrapolate the steady-state nucleation rate $J_{ss}(T)$ [Eq. (A2) or (A5)] to larger undercoolings, the viscosity η has to be known over the entire temperature range. η is approximated by a Vogel-Fulcher-Tammann ansatz[11]

$$\eta(T) = \eta_0 \exp\left(\frac{A}{T - T_0}\right) \tag{1}$$

under three constraints. (i) $\eta(T_l)=2\times10^{-2}$ poise as used above for small undercoolings. (ii) $\eta(T_g)=10^{13}$ poise, which is commonly used to define the glass transition.[11] As pointed out in Ref. 38, T_g can be chosen to be close to the crystallization temperature in furnace heating experiments:[3–5,10,38,49,50] $T_g=195$ °C ($Ge_{12}Sb_{88}$), $T_g=170$ °C (AgIn–Sb_2Te), $T_g=190$ °C ($Ge_4Sb_1Te_5$), and $T_g=155$ °C ($Ge_2Sb_2Te_5$). (iii) The fragility index as defined by Angell[51]

$$m = \left.\frac{\partial \log_{10} \eta(T)}{\partial (T_g/T)}\right|_{T=T_g} \tag{2}$$

was matched to literature values[52–54] for various chalcogenides by setting $m=45$. These constraints yielded reasonable activation energies for the viscosity of about 4 eV at T_g. The steady-state nucleation rate $J_{ss}(T)$ [Eq. (A5)] obtained this way is plotted in Fig. 3 for both the TS and the HM approximation. J_{ss} increases rapidly for small undercoolings. This explains why the nucleation temperature T_n (Table I) was observed to be independent of cooling rate and sample volume within the range given in Sec. II. Nucleation can only occur once the observable limit on the order of 1 $mm^{-3}\,s^{-1}$ is exceeded, i.e., one nucleation event in a typical sample volume of about 1 mm^3 during the observable time window of 1 s. The height and the position of the maximum in J_{ss} (Fig. 3) depend only weakly on the choice of the glass transition temperature T_g and the fragility index m in the constraints above. If T_g is varied as ∓40 °C or if m is varied as ±15, the height changes by about ±1 order of magnitude and the position by about ±0.01. The more pronounced contribution to the uncertainty in the maximum height is that of the nucleation rate prefactor J_0 [Eq. (A2)], i.e., about two to four orders of magnitude.[46] The part of the curve to the left of the maximum is essentially insensitive to those uncertainties. Since we did not establish that nucleation was homogeneous in our experiments, the nucleation rate J_{ss} as plotted in Fig. 3 is an upper limit for the homogeneous nucleation rate. We refrain from plotting J_{ss} for undercoolings larger than $\Delta T_r=0.4$ for two reasons: (a) The free energy approximations [Eq. (A3)] are increasingly imprecise for larger undercoolings. (b) There are indications[55,56] that the Stokes-Einstein equation, which allowed us to express the preexponential factor in Eq. (A2) in terms of the viscosity η, may not hold for temperatures around T_g, which corresponds to an undercooling of about $\Delta T_r=0.5$.

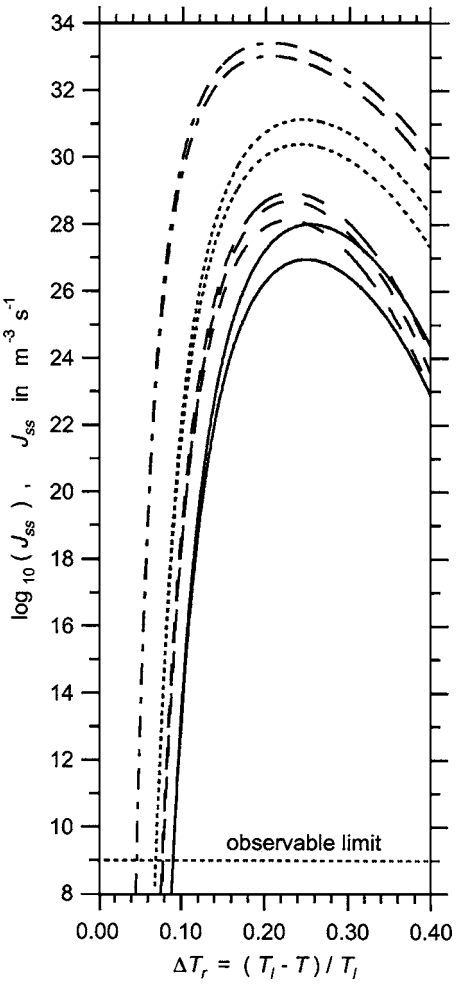

FIG. 3. Upper limit for the homogeneous steady-state crystal nucleation rate J_{ss} [Eq. (A5)] as a function of relative undercooling ΔT_r [Eq. (A4)] for $Ge_2Sb_2Te_5$ (dot-dashed), $Ge_4Sb_1Te_5$ (dotted), AgIn–Sb_2Te (dashed), and $Ge_{12}Sb_{88}$ (solid). For each alloy, the upper curve corresponds to the TS approximation and the lower curve to the HM approximation of the Gibbs free energy [cf. Eq. (A3)]. For AgIn–Sb_2Te, the intermediate curve corresponds to the Gibbs free energy approximation from Ref. 38. For all alloys, nucleation is observed if J_{ss} exceeds about 1 $mm^{-3}\,s^{-1}$ (observable limit); the corresponding undercoolings $\Delta T_{n,r}$ are those of Table I.

V. DISCUSSION

A. Crystallization

At fixed undercooling ΔT_r, the steady-state nucleation rate J_{ss} [Eq. (A5)] depends critically only on three parameters: the normalized interfacial energy α, the entropy of fusion β, and the reduced glass transition temperature $T_{rg}=T_g/T_l$. The latter determines the degree of undercooling ΔT_r at which the viscosity η constrains the nucleation rate to decrease on the right side of the maximum.[42] At fixed undercooling ΔT_r, J_{ss} decreases with increasing parameters α, β, and T_{rg} [Eq. (A5)]. According to the analysis in Sec. IV (also cf. Ref. 38), $T_{rg}=0.53$ ($Ge_{12}Sb_{88}$), $T_{rg}=0.55$ ($AgIn-Sb_2Te$), $T_{rg}=0.48$ ($Ge_4Sb_1Te_5$), and $T_{rg}=0.47$ ($Ge_2Sb_2Te_5$). The parameters β (Table I) and T_{rg} are higher for the Sb-rich alloys than for GeSbTe alloys, which causes a higher nucleation rate for the latter (Fig. 3). The nucleation rate is highest for $Ge_2Sb_2Te_5$ due to its lower value of α (Table I), which affects the exponential part of the nucleation rate by a power of 3 [Eq. (A5)].

Studies on the recrystallization mechanism of amorphous marks upon laser irradiation revealed that $Ge_4Sb_1Te_5$ and $Ge_2Sb_2Te_5$ recrystallize by nucleation and subsequent growth of crystals inside the amorphous mark.[57] In contrast, $Ge_{12}Sb_{88}$ and $AgIn-Sb_2Te$ recrystallize by the growth of the crystalline phase from the rim of the amorphous mark.[10,58] This correlates with our findings of a lower nucleation rate for the Sb-rich alloys than for the GeSbTe alloys and is finally related to the relative difference in the parameters α, β, and T_{rg} among these alloys.

It should be noted, however, that the nucleation rates given in Fig. 3 and the crystal-melt interfacial energies σ and α given in Table I strictly apply only to that crystal phase that actually nucleated in the undercooling experiments. For the $Ge_2Sb_2Te_5$ alloy, this is probably not the metastable cubic phase, which is found following laser-induced crystallization,[59] but the hexagonal phase, which is the stable phase,[4,60] which forms upon furnace heating the cubic phase above about 300 °C. For an estimate of the crystal-melt interfacial energy for the cubic phase for $Ge_2Sb_2Te_5$, the undercooling should be measured from the (unknown) liquidus temperature of the cubic phase, which should be lower than the (measured) liquidus temperature of the hexagonal phase. Moreover, the (unknown) heat of fusion for the cubic phase would have to be used for the free energy approximation [Eq. (A3)].

B. Amorphization

The steady-state nucleation rates given in Fig. 3 are too high to allow amorphization in both optical and electronic media under operating conditions. Nucleation interferes at the highest attainable cooling rates, which can be estimated by dimensional analysis of the heat conduction equation.[61] The minimum time for heat removal by conduction is on the order of

$$\tau=\frac{l^2 c^{(\nu)}}{\lambda}, \tag{3}$$

where l is the shortest dimension of an amorphous mark, which is at best on the order of 10 nm (film thickness for optical media and minimum programmable volume dimension for electronic media). λ and $c^{(\nu)}$ are the thermal conductivity and specific heat per volume, respectively, which are on the order of $0.2\ \mathrm{W\,m^{-1}\,K^{-1}}$ and $1.3\times10^6\ \mathrm{J\,m^{-3}\,K^{-1}}$, respectively.[2,38,62,63] This yields $\tau\sim1$ ns, which implies that the highest attainable cooling rate is on the order of $10^{10}\ \mathrm{K\,s^{-1}}$. Consistently, such cooling rates were obtained by more accurate modeling of temperature profiles.[62] For optical data storage, the bit volume[64] is on the order of $V_b=1\ \mu\mathrm{m}\times1\ \mu\mathrm{m}\times10\ \mathrm{nm}=10^{-20}\ \mathrm{m^3}$ (limited by the wavelength of the laser light). For a cooling rate of $10^{10}\ \mathrm{K\,s^{-1}}$, the temperature decreases by 100 K over a time of $t_c=10\ \mathrm{ns}=10^{-8}$ s. Therefore, nucleation would interfere if the nucleation rate were $J_{ss}>V_b^{-1}t_c^{-1}=10^{28}\ \mathrm{m^{-3}\,s^{-1}}$ over a range of 100 K. This is certainly the case for the GeSbTe alloys (Fig. 3), but most likely also for the Sb-rich alloys, since the nucleation rates determined by the fluxing technique probably approached the limit of homogeneous nucleation far closer than the nucleation rates in phase change media, which are even enhanced by nucleation-promoting dielectric capping layers.[65,66] For electronic media, programmable volume sizes as small as $V_b=10^{-23}\ \mathrm{m^3}$ are reported.[67,68] Hence, nucleation would interfere if $J_{ss}>10^{31}\ \mathrm{m^{-3}\,s^{-1}}$ over a range of 100 K, which is at least the case for $Ge_2Sb_2Te_5$, which is often reported as the material of choice for PC-RAM prototypes.[2] Therefore, we conclude that: (i) Melt quenching under operating conditions occurs during the incubation time, when the steady-state distribution of critical nuclei is not yet formed,[12,46,69] so that the nucleation rate remains far smaller than its steady-state value J_{ss}. As the incubation time is independent of the bit volume V_b, this statement applies equally to optical and electronic media for all alloys investigated. Consistently, it was reported by Kelton and Greer[70] that transient effects become increasingly important with increasing quench rate: While the steady-state nucleation rate is readily maintained for cooling rates on the order of $1\ \mathrm{K\,s^{-1}}$ as used in the present experiments or in conventional metallurgical solidification, deviations from the steady state are already large at cooling rates in rapid solidification techniques, such as melt spinning ($\sim10^6\ \mathrm{K\,s^{-1}}$), and must be even larger for cooling rates under operating conditions of phase change media. (ii) Amorphization would not be possible if the incubation time were absent. Hence, the existence of an incubation time makes phase change recording possible. This statement should apply for optical data storage to all alloys investigated and for electronic data storage at least to $Ge_2Sb_2Te_5$. Indeed, incubation times were reported upon crystallization on the time scale of minutes[6,7,71,72] around T_g, as well as upon laser crystallization on the nanosecond time scale.[57,59,73,74]

VI. CONCLUSIONS

(1) B_2O_3 is an effective flux to enhance the undercooling of liquid Sb and Te alloys.

(2) The steady-state nucleation rate was higher for the GeSbTe alloys than for the Sb-rich alloys. This is attributed to the molar entropy of fusion β and the reduced glass transition temperature T_g/T_l, both of which are higher for the Sb-rich alloys. The lower value of the (normalized) interfacial energy α for $Ge_2Sb_2Te_5$ caused an additional increase in the nucleation rate for this alloy. The observations are qualitatively in agreement with the different kinetics of crystallization of the four alloys observed under laser irradiation.
(3) The presence of an incubation time makes phase change recording possible for both optical and electronic media.
(4) The nucleation parameters determined in this work can be used to model crystallization kinetics.

ACKNOWLEDGMENTS

One of the authors (J.K.) acknowledges the Deutscher Akademischer Austauschdienst and the Studienstiftung des Deutschen Volkes for financial support. Another author (F.S.) acknowledges partial support from the Alexander-von-Humboldt-Stiftung. H. Dieker is acknowledged for providing the starting materials. Work at Harvard is supported in part by the MRSEC program of the NSF.

APPENDIX: DETERMINATION OF THE INTERFACIAL ENERGY FROM OBSERVATIONS DURING CONTINUOUS COOLING

Nucleation at a steady-state rate J_{ss} of a new phase in an undercooled liquid of volume V cooled at a rate $\dot{T}<0$ leads to transformation if the probability of nucleation during cooling from the liquidus temperature T_l to the nucleation temperature T_n is unity,[17]

$$\frac{V}{\dot{T}}\int_{T_l}^{T_n} J_{ss}(T)dT \sim 1. \tag{A1}$$

The steady-state nucleation rate J_{ss} is given by the classical theory of nucleation,[46]

$$J_{ss}(T) = \frac{J_0}{\eta(T)} \exp\left[-\frac{16\pi}{3k_BT}\frac{\sigma^3}{(\Delta G_V)^2}f(\theta)\right] \quad \mathrm{m^{-3}\,s^{-1}}, \tag{A2}$$

where η is the viscosity of the melt (in poise), σ the crystal-melt interfacial energy, ΔG_V the difference in Gibbs free energy between undercooled liquid and crystal per unit volume, and $f(\theta)\leqslant 1$ a heterogeneous nucleation reduction factor. For condensed systems, nucleation theory predicts $J_0=10^{36}$, with an uncertainty between two to four orders of magnitude.[17,35,42,46,75–78] When liquid heat-capacity data are not available, ΔG_V has to be estimated. Simple approximations were proposed by Turnbull[41] (TB), Thompson and Spaepen[39] (TS), and Hoffman[40] (HM):

$$\Delta G_V = \Delta H_{f,V}\frac{T_l - T}{T_l} \equiv \phi \quad \text{(TB)},$$

$$\Delta G_V = \phi\frac{2T}{T_l + T} \quad \text{(TS)},$$

$$\Delta G_V = \phi\frac{T}{T_l} \quad \text{(HM)}, \tag{A3}$$

where $\Delta H_{f,V}$ is the heat (enthalpy) of fusion per unit volume. Dimensionless parameters are defined by[42]

$$\alpha = \frac{\sigma\Omega^{2/3}}{\Delta H_{f,m}/N_{\mathrm{Av}}} = \frac{(N_{\mathrm{Av}}V_m^2)^{1/3}\sigma}{\Delta H_{f,m}}, \quad \beta = \frac{\Delta H_{f,m}}{RT_l},$$

$$T_r = \frac{T}{T_l}, \quad \Delta T_r = \frac{T_l - T}{T_l}, \tag{A4}$$

where α is the interfacial energy per atomic area in the interface, normalized by the heat of fusion per atom; it is a measure for the number of monolayers that can be melted with the interfacial energy. $\Delta H_{f,m}$ is the molar heat of fusion, and β an entropy of fusion, normalized to the gas constant R. N_{Av}, Ω, and V_m are Avogadro's number, the atomic volume, and the molar volume, respectively. This yields the steady-state nucleation rate as a function of dimensionless parameters:

$$J_{ss}(T) = \frac{10^{36}}{\eta(T)} \times \exp\left[-\frac{16\pi}{3}\frac{f(\theta)}{T_r(\Delta T_r)^2}\alpha^3\beta\right] \quad \mathrm{m^{-3}\,s^{-1}} \quad \text{(TB)},$$

$$J_{ss}(T) = \frac{10^{36}}{\eta(T)} \times \exp\left[-\frac{4\pi}{3}\frac{(T_r+1)^2 f(\theta)}{T_r(\Delta T_r)^2}\alpha^3\beta\right] \quad \mathrm{m^{-3}\,s^{-1}} \quad \text{(TS)},$$

$$J_{ss}(T) = \frac{10^{36}}{\eta(T)} \times \exp\left[-\frac{16\pi}{3}\frac{f(\theta)}{T_r^3(\Delta T_r)^2}\alpha^3\beta\right] \quad \mathrm{m^{-3}\,s^{-1}} \quad \text{(HM)}. \tag{A5}$$

It is instructive to set $f(\theta)=1$ and thereby assume that nucleation in the undercooling experiments was homogeneous.[14,15,17] Hence, substitution of Eq. (A2) or Eq. (A5) into Eq. (A1) and numerical evaluation of the integral yield an estimate for the interfacial energy if the heat of fusion ΔH_f and the viscosity η are known. In case nucleation was heterogeneous, this analysis still yields a lower limit for the interfacial energy and an upper limit for the *homogeneous* steady-state nucleation rate.

[1] N. Yamada, MRS Bull. **21**, 48 (1996).
[2] S. Hudgens and B. Johnson, MRS Bull. **29**, 829 (2004).
[3] D. Wamwangi, W. K. Njoroge, and M. Wuttig, Thin Solid Films **408**, 310 (2002).
[4] I. Friedrich, V. Weidenhof, W. Njoroge, P. Franz, and M. Wuttig, J. Appl. Phys. **87**, 4130 (2000).
[5] W. K. Njoroge and M. Wuttig, J. Appl. Phys. **90**, 3816 (2001).
[6] G. Ruitenberg, A. K. Petford-Long, and R. C. Doole, J. Appl. Phys. **92**, 3116 (2002).
[7] S. Privitera, C. Bongiorno, E. Rimini, and R. Zonca, Appl. Phys. Lett. **84**, 4448 (2004).
[8] B. J. Kooi and J. Th. M. De Hosson, J. Appl. Phys. **95**, 4714 (2004).

[9]J. Kalb, F. Spaepen, and M. Wuttig, Appl. Phys. Lett. **84**, 5240 (2004).
[10]L. van Pieterson, M. van Schijndel, J. C. N. Rijpers, and M. Kaiser, Appl. Phys. Lett. **83**, 1373 (2003).
[11]R. H. Doremus, *Glass Science*, 2nd ed. (Wiley, New York, 1994).
[12]K. F. Kelton, Solid State Phys. **45**, 75 (1991).
[13]H. W. Kui, A. L. Greer, and D. Turnbull, Appl. Phys. Lett. **45**, 615 (1984).
[14]G. Devaud and D. Turnbull, Appl. Phys. Lett. **46**, 844 (1985).
[15]H. W. Kui and D. Turnbull, Appl. Phys. Lett. **47**, 796 (1985).
[16]C. F. Lau and H. W. Kui, J. Appl. Phys. **67**, 3181 (1990).
[17]Y. Shao and F. Spaepen, J. Appl. Phys. **79**, 2981 (1996).
[18]T. D. Shen and R. B. Schwarz, Appl. Phys. Lett. **75**, 49 (1999).
[19]D. M. Herlach, D. Holland-Moritz, Th. Schenk, K. Schneider, G. Wilde, O. Boni, J. Fransaer, and F. Spaepen, J. Non-Cryst. Solids **250–252,** 271 (1999).
[20]J. F. Elliott and M. Gleiser, *Thermochemistry for Steelmaking* (Addison-Wesley, London, 1960).
[21]W. T. Laughlin and D. R. Uhlmann, J. Phys. Chem. **76**, 2317 (1972).
[22]A. I. Priven, Glass Phys. Chem. **26**, 541 (2000).
[23]M. J. Aziz, Ph.D. thesis, Harvard University, 1983.
[24]G. W. H. Höhne, H. K. Cammenga, W. Eysel, E. Gmelin, and W. Hemminger, Thermochim. Acta **160**, 1 (1990).
[25]H. K. Cammenga, W. Eysel, E. Gmelin, W. Hemminger, G. W. H. Höhne, and S. M. Sarge, Thermochim. Acta **219**, 333 (1993).
[26]S. M. Sarge, E. Gmelin, G. W. H. Höhne, H. K. Cammenga, W. Hemminger, and W. Eysel, Thermochim. Acta **247**, 129 (1994).
[27]S. M. Sarge, G. W. H. Höhne, H. K. Cammenga, W. Eysel, and E. Gmelin, Thermochim. Acta **361**, 1 (2000).
[28]*Binary Alloy Phase Diagrams*, edited by T. Massalski, 2nd ed. (American Society for Metals, Metals Park, OH, 1990).
[29]V. Weidenhof, I. Friedrich, S. Ziegler, and M. Wuttig, J. Appl. Phys. **86**, 5879 (1999).
[30]N. Kh. Abrikosov and G. T. Danilova-Dobryakova, Izv. Akad. Nauk SSSR, Neorg. Mater. **1**, 204 (1965).
[31]B. Legendre, C. Hancheng, S. Bordas, and M. T. Clavaguera-Mora, Thermochim. Acta **78**, 141 (1984).
[32]S. Bordas, M. T. Clavaguera-Mora, B. Legendre, and C. Hancheng, Thermochim. Acta **107**, 239 (1986).
[33]R. E. Cech and D. Turnbull, J. Met. **191**, 242 (1951).
[34]J. H. Perepezko, *Proceedings of the Second International Conference on Rapid Solidification Processing*, Reston, VA, edited by R. Mehrabian, B. H. Kear, and M. Cohen (Claitor's, Baton Rouge, LA, 1980), p. 56.
[35]C. V. Thompson and F. Spaepen, Acta Metall. **31**, 2021 (1983).
[36]J. H. Perepezko, Mater. Sci. Eng. **65**, 125 (1984).
[37]D. H. Rasmussen, J. H. Perepezko, and C. R. Loper, *Proceedings of the Second International Conference on Rapidly Quenched Metals*, edited by N. J. Grant and B. C. Giessen (Massachusetts Institute of Technology Press, Cambridge, 1976), Vol. 1, p. 51.
[38]J. Kalb, F. Spaepen, and M. Wuttig, J. Appl. Phys. **93**, 2389 (2003).
[39]C. V. Thompson and F. Spaepen, Acta Metall. **27**, 1855 (1979).
[40]J. D. Hoffman, J. Chem. Phys. **29**, 1192 (1958).
[41]D. Turnbull, J. Appl. Phys. **21**, 1022 (1950).
[42]D. Turnbull, Contemp. Phys. **10**, 473 (1969).
[43]F. Herwig and M. Wobst, Z. Metallkd. **83**, 35 (1991).
[44]F. Herwig and M. Wobst, Z. Metallkd. **82**, 917 (1991).
[45]H. Neumann, F. Herwig, and W. Hoyer, J. Non-Cryst. Solids **205–207**, 438 (1996).
[46]J. W. Christian, *The Theory of Transformations in Metals and Alloys*, 2nd ed. (Pergamon, North-Holland, Amsterdam, 1975).
[47]F. Spaepen and R. B. Meyer, Scr. Metall. **10**, 257 (1976).
[48]C. V. Thompson, Ph.D. thesis, Harvard University, 1981.
[49]T. Okabe, S. Endo, and S. Saito, J. Non-Cryst. Solids **117–118**, 222 (1990).
[50]A. K. Petford-Long, R. C. Doole, C. N. Afonso, and J. Solis, J. Appl. Phys. **77**, 607 (1995).
[51]C. A. Angell, J. Non-Cryst. Solids **73**, 1 (1985).
[52]U. Senapati and A. K. Varshneya, J. Non-Cryst. Solids **197**, 210 (1996).
[53]A. S. Tverjanovich, J. Non-Cryst. Solids **298**, 226 (2002).
[54]A. S. Tverjanovich, Glass Phys. Chem. **29**, 532 (2003).
[55]J. A. Hodgdon and F. H. Stillinger, Phys. Rev. E **48**, 207 (1993).
[56]P. G. Debenedetti and F. H. Stillinger, Nature (London) **410**, 259 (2001).
[57]J. H. Coombs, A. P. J. M. Jongenelis, W. van Es-Spiekman, and B. A. J. Jacobs, J. Appl. Phys. **78**, 4918 (1995).
[58]H. J. Borg, M. van Schijndel, J. C. N. Rijpers, M. H. R. Lankhorst, G. Zhou, M. J. Dekker, I. P. D. Ubbens, and M. Kuijper, Jpn. J. Appl. Phys., Part 1 **40**, 1592 (2001).
[59]I. Friedrich, V. Weidenhof, S. Lenk, and M. Wuttig, Thin Solid Films **389**, 239 (2001).
[60]N. Yamada, E. Ohno, K. Nishiuchi, N. Akahira, and M. Takao, J. Appl. Phys. **69**, 2849 (1991).
[61]H. S. Carslaw and J. C. Jaeger, *Conduction of Heat in Solids*, 2nd ed. (Clarendon, Oxford, 1959).
[62]C. Peng, L. Cheng, and M. Mansuripur, J. Appl. Phys. **82**, 4183 (1997).
[63]E.-K. Kim, S.-I. Kwun, S.-M. Lee, H. Seo, and J.-G. Yoon, Appl. Phys. Lett. **76**, 3864 (2000).
[64]M. Kaiser, L. van Pieterson, and M. A. Verheijen, J. Appl. Phys. **96**, 3193 (2004).
[65]N. Ohshima, J. Appl. Phys. **79**, 8357 (1996).
[66]W. K. Njoroge, H. Dieker, and M. Wuttig, J. Appl. Phys. **96**, 2624 (2004).
[67]M. H. R. Lankhorst, B. W. S. M. M. Ketelaars, and R. A. M. Wolters, Nat. Mater. **4**, 347 (2005).
[68]P. Haring Bolivar, F. Merget, D.-H. Kim, B. Hadam, and H. Kurz, European Symposium on Phase Change and Ovonic Science, Balzers, Liechtenstein, 2004 (unpublished).
[69]D. T. Wu, Solid State Phys. **50**, 37 (1997).
[70]K. F. Kelton and A. L. Greer, J. Non-Cryst. Solids **79**, 295 (1986).
[71]Q. M. Lu and M. Libera, J. Appl. Phys. **77**, 517 (1995).
[72]J. A. Kalb, C. Y. Wen, F. Spaepen, H. Dieker, and M. Wuttig, J. Appl. Phys. **98**, 054902 (2005).
[73]V. Weidenhof, I. Friedrich, S. Ziegler, and M. Wuttig, J. Appl. Phys. **89**, 3168 (2001).
[74]H.-W. Wöltgens, R. Detemple, I. Friedrich, W. K. Njoroge, I. Thomas, V. Weidenhof, S. Ziegler, and M. Wuttig, Mater. Res. Soc. Symp. Proc. **674**, V1.3 (2001).
[75]D. Turnbull and J. C. Fisher, J. Chem. Phys. **17**, 71 (1949).
[76]D. Turnbull, J. Chem. Phys. **20**, 411 (1952).
[77]F. Spaepen and D. Turnbull, *Proceedings of the Second International Conference on Rapidly Quenched Metals*, edited by N. J. Grant and B. C. Giessen (Massachusetts Institute of Technology Press, Cambridge, 1976), Vol. 1, p. 205.
[78]F. Spaepen, Mater. Res. Soc. Symp. Proc. **57**, 161 (1986).

January 22, 2006

LIST OF ERRATA [J. Appl. Phys. 98, 054910 (2005)]:

1. The uncertainty in the normalized interfacial energy α for the alloy $Ge_4Sb_1Te_5$ in Table I was not listed correctly in the published article.
   The article states $\alpha = 0.22 \pm 0.01$. The correct value is $\alpha = 0.22 \pm 0.02$.

2. An exponent of (-1) is missing in the (TS) approximation in Eq. (A5).
   The published article states:

$$J_{ss}(T) = \frac{10^{36}}{\eta(T)} \times \exp\left(-\frac{4\pi}{3} \cdot \frac{(T_r + 1)^2 f(\theta)}{T_r (\Delta T_r)^2} \cdot \alpha^3 \beta \right) \quad \text{m}^{-3}\,\text{s}^{-1} \qquad \text{(TS)} \quad \text{(A5)}.$$

   The correct expression is:

$$J_{ss}(T) = \frac{10^{36}}{\eta(T)} \times \exp\left(-\frac{4\pi}{3} \cdot \frac{(T_r^{-1} + 1)^2 f(\theta)}{T_r (\Delta T_r)^2} \cdot \alpha^3 \beta \right) \text{m}^{-3}\,\text{s}^{-1} \qquad \text{(TS)} \quad \text{(A5)}.$$

   [Note the additional exponent of (-1) in the numerator of the exponential part.]
   The data analysis in the published article was however based on the correct equation.